Journal of Ovonic Research Vol. 16, No. 4, July - August 2020, p. 189 - 196

COMPARATIVE ANALYSIS OF ELECTRON DIFFRACTION PATTERN OBTAINED WITHOUT AND WITH PRECESSION SYSTEM

R. MANU[a,*], V. CIUPINA[a,b,c], G. PRODAN[b]
[a]*Doctoral School of Physics, University of Bucharest, Atomistilor No. 405, 077125, Magurele, Romania*
[b]*Ovidius University of Constanta, Mamaia Avenue No. 124, 900527, Constanta, Romania*
[c]*Accademy of Romanian Scientists, Splaiul Independentei No. 54, 050094, Bucharest, Romania*

Electron diffraction is an additional technique in electronic microscopy studies. Since the XRD or neutron diffraction techniques was used intensely for crystalline structure determination, electron diffraction has potential for special cases were even this technique fails. Due to several factor the electron diffraction is not suitable for crystal structure determination, but with hardware and software improvement we can transform this technique in useful one. We show here an example of analysis of five different samples using combined technique, such as TEM/HRTEM image, electron diffraction without and with improvement provided by a precession system. We highlight the cases were electron diffraction succeed and the cases were failed, even the precession system is used.

(Received March 11, 2020; Accepted July 6, 2020)

Keywords: TEM, HRTEM, Electron diffraction, Precession, Scherrer

1. Introduction

Electron diffraction is an additional technique in electronic microscopy studies. This technique was not imposed due to difficulties to obtained reliable data for all sample, so the processing step are dependent on several factors, which depend on both the instrument and the samples examined. However, the diffraction of electrons can be useful in many situations. Thus, by adding appropriate processing techniques we can improve the results achieved. Data processing techniques can be retrieved from applications developed for X-ray diffraction, adjusting the mathematical apparatus. A special technique in the case of electron diffraction is the precession of electron diffraction. It is a technique introduced by the point in 1994 by Vincent and Midgley [1] and later developed by C. Own [2].

Among the advantages of using the precession of electron diffraction in the acquisition of diffraction patterns we can include: reducing the dependence of the intensities by the thickness of the sample, reducing the effects due to the Ewald sphere, reducing dynamic effects, can be installed on a very wide range of instruments, even older versions, without the need for special configurations. Using the precession of electron diffraction, we can obtain diffraction figures with low dynamic effects; intensities extracted from these figures can then be used in the study of the crystalline structure. Diffractions obtained on polycrystalline materials are disturbed using stop beam covering the central spot to protect the camera's scintillator from too strong exposure. Using the precession of electron diffraction and an appropriate geometry of objective apertures and selecting the range can obtain a figure of diffraction in which there is no need to use stop beam.

The purpose of this work is to highlight the usefulness of the precession of electron diffraction in different situations, differentiated by the type of samples examined, namely: amorphous materials, crystalline materials, polycrystalline materials with cubic and hexagonal structure, complex materials (mixed phases: crystalline, amorphous).

[*] Corresponding author: raducumanu@gmail.com

2. Experimental

Five samples were selected for the experiment, with different characteristics, both morphologically and crystalline. The purpose of this selection was to test the influence of the extinction distance of the diffracted beam in these samples. It also highlights the need to use the precession system.

The preparation of the samples was carried out in such a way as to avoid the introduction of artifacts, defects or changes in the initial sample. Thus, for nanoparticles, a dilution was carried out in alcohol, from which a drop was taken on the TEM grid, covered with formvar. For thin films, the quick method [3] was chosen. In this case there is a risk of defects in the film, but they can be avoided by means of selecting suitable area from the preview using TEM images.

The Philips CM120ST electron microscope with an acceleration voltage of 100kV was used for investigations. TEM images help characterize morphologically and select the work area to retrieve diffraction figures. In all cases, areas were selected using the selection aperture in the microscope column. After taking over the classical diffraction figure, the precession system was activated, properly aligned before the data capture operations. The precession of electron diffraction is an examination procedure obtained using the NanoMegas SpinningStar P020 system. First, the electron beam is deflected and rotated using the condenser lens. The frequency of rotation is a controllable parameter using electronic equipment. After interacting with the studied material, it is coiled using DeScan lenses. The precession of electron diffraction is equivalent to the method of the rotating crystal used in the diffraction of x-rays. In Fig. 1 is schematically represented the principle of precession of electron diffraction.

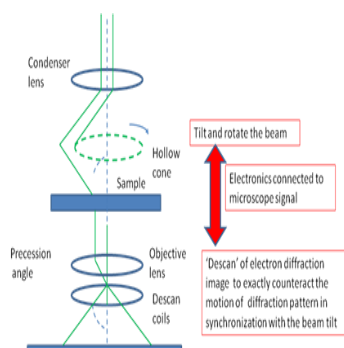

Fig. 1. The precession of electron diffraction.

The acquisition of TEM images and diffraction figures was made in the iTEM platform, which allows the acquisition of images with the working information of the microscope: magnification/camera length, lens currents, (X, Y, Z, α, β) sample position.

The processing of diffraction figures was carried out in the CRISP2 application [4], with the specialized ELD [5] module for polycrystalline diffraction. The results obtained using ELD are peaks position and FWHM (Full Width at Half Maximum) extracted from the calculated profile from the diffraction pattern. The position of the peaks is given as interplanar distances and can be easily converted in diffraction angle. These values help to confirm the crystalline structure of the sample. An indexing of these peaks can also be achieved, but the procedure is quite complex and is not relevant to our experiment. The FWHM allows Scherrer analysis [6] for that sample, showing its characteristic crystals dimension:

$$D_S = \frac{k \cdot \lambda}{\beta \cdot cos\theta}$$

where D_S is the size of the crystals dimension, k a constant (k=0.9) [7], λ the wavelength associated with the electron beam (0.0037nm at 100kV), the β FWHM, θ the scattering angle.

To highlight the differences, we exported extracted profiles in the form of ASCII data, and represented the profiles obtained for electron diffraction without or with precession system, in the same graph. For graphic construction we used the FitYK, that allows analysis of diffraction profiles, where we can turn data into a more easy-to-interpret format, for example (x, y) point sets. Keeping only the minimum evolution range for the two profiles, as in ELD the area selected for analysis may vary depending on the centering of the diffraction figure in the captured image.

The data obtained were imported into SciDAVIS and translated as graphs for an intuitive interpretation, together with data obtained from the X-ray diffraction on those samples [8]. The Mott-Bethe formula [9] show the relation between the atomic scattering factor for the electron and atomic scattering factor of the X-ray diffraction.

$$f(s) = \frac{m_0 \cdot e^2}{8\pi^2 \hbar^2} \cdot \frac{1}{4\pi\varepsilon_0} \cdot \frac{Z - f^X(s)}{s^2}$$

where: $s = \frac{sin\theta}{\lambda}$, Z atomic number, m_0 electron rest mass, e electron charge, $\varepsilon_0$vacuum permitivity, f^Xatomic scattering factor for X-rays.

$$f(s) = a - b \cdot f^X(s)$$

The intensity of diffracted beam will depend on the structure factor that can be calculated when the crystalline structure is known. If we consider a proportional link between the structure factor and the atomic scattering factor, we come to:

$$F(s) = k \cdot f(s) = k \cdot \left(a - b \cdot f^X(s)\right)$$

and the intensity of the diffracted beam will be:

$$I(s) = F(s) \cdot F^*(s) = k^2 \cdot f^2(s)$$

If we graphically represent the intensities of diffracted electron beams and the intensities of XRD diffraction, we can visually compare the evolution of intensities in the two techniques of diffraction of electrons: classical and using the precession system. Establishing an analytical relationship to track this evolution is complex, because in the case of materials with multiple elements the structure factor will have a complex dependence on the scattering factor, such as the cubic structure, or hexagonal CdS.

3. Results

Fig. 2 shows the TEM images of the five samples. In each TEM image, the diffraction figures were inserted for the two working modes: without (left) and with precession (right). We try also to eliminate the stop beam using special technique presented above. One issue in applying this technique is the lost of calibration, so for each figure acquired, recalibration is necessary. This can be observed in the case of Al sample were interplanar distance are lower than correct value. In some cases, this can be adjusted by simple shift operation applied to values.

Fig. 3 shows features profiles extracted from diffraction figures. It should be noted that the intensities used in the construction of the graphs shown in Fig. 3 are determined by the ELD module after the extraction of the background noise automatically identified. To minimize profile matching errors calculated based on the identified peaks, additional peaks can be added, but they may or may not be associated with that sample. The so-called ghost peaks help to achieve good fit, but in some cases, they are difficult to interpret.

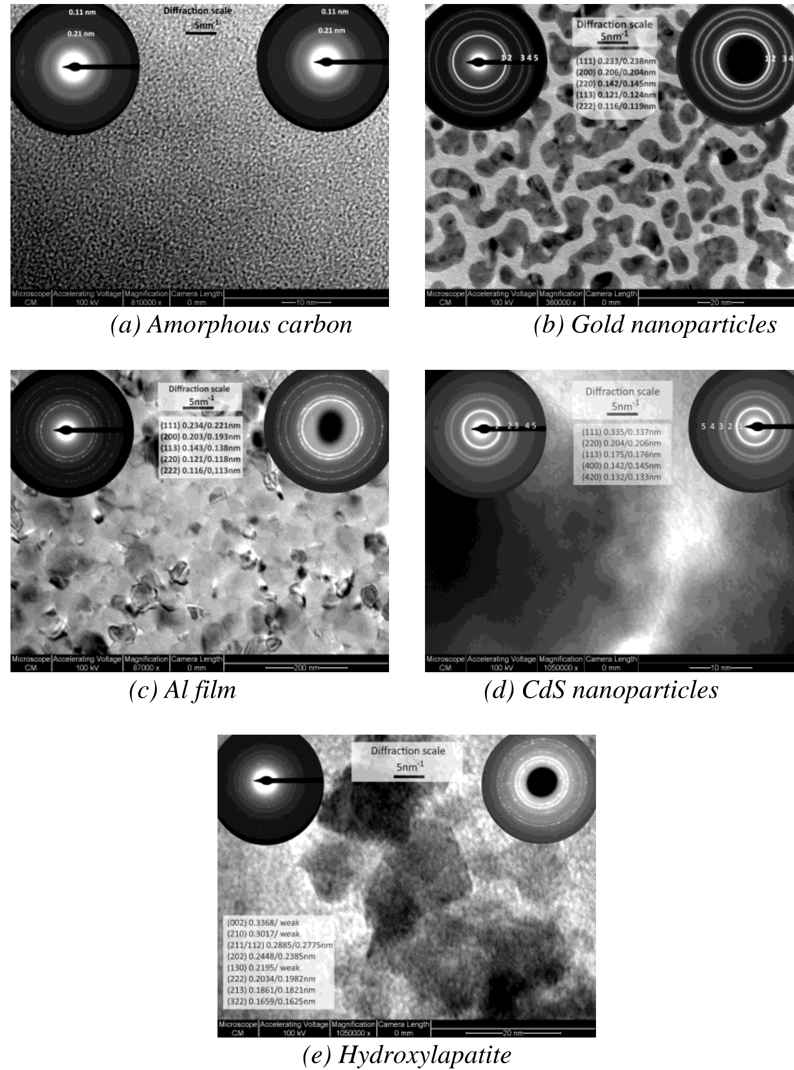

(a) Amorphous carbon *(b) Gold nanoparticles*

(c) Al film *(d) CdS nanoparticles*

(e) Hydroxylapatite

Fig. 2. TEM images of the samples examined. Inserted are diffraction figures obtained without (left) and with precession system active (right).
(a) Amorphous carbon; (b) Gold nanoparticles; (c) Al film; (d) CdS nanoparticles;(e) Hydroxylapatite

Table 1. Crystals dimension from Scherrer's formula.

Sample	dhkl	Classic (nm)	Precession (nm)
Amorphous carbon	0.21 nm	1.9856	1.9130
	0.11 nm	1.9130	1.7651
	Mean value	1.8729	1.8391
Gold nanoparticles	(111) 0.233/0.238nm	8.1725	7.3337
	(200) 0.206/0.204nm	7.6883	7.5122
	(220) 0.142/0.145nm	6.0941	6.3665
	(113) 0.121/0.124nm	6.6604	6.9481
	(222) 0.116/0.119nm	6.1011	6.3744
	Mean value	6.9433	6,9070
Al film	(111) 0.234/0.221nm	9.8673	7.3737
	(200) 0.203/0.193nm	9.2570	6.7591
	(220) 0.143/0.138nm	9.2317	8.6395
	(113) 0.121/0.118nm	13.3697	6.3381
	(222) 0.116/0.113nm	12.2615	5.7733
	Mean value	10.7974	6.9767
CdS nanoparticles	(111) 0.335/0.337nm	4.5808	4.2610

Sample	dhkl	Classic (nm)	Precession (nm)
	(220) 0.204/0.206nm	4.6816	4.2241
	(113) 0.175/0.176nm	4.5785	3.9799
	(400) 0.142/0.145nm	4.5375	3.1709
	(420) 0.132/0.133nm	3.9185	3.1835
	Mean value	4.4594	3.7639
Hydroxylapatite	(002) 0.3368nm/ weak	6.0014	-
	(210) 0.3017nm/ weak	5.8494	-
	(211/112) 0.2885/0.2775nm	6.2379	5.7714
	(202) 0.2448/0.2385nm	5.9885	5.6846
	(130) 0.2195nm/ weak	6.1922	-
	(222) 0.2034/0.1982nm	6.2023	5.8933
	(213) 0.1861/0.1821nm	6.2332	5.9688
	(322) 0.1659/0.1625nm	6.1876	5.9430
	Mean value	6.1116	5.8522

4. Discussions

Fig. 2a shows the carbon amorphous film chosen for study, film obtained by TVA method. The substrate used for this experiment was Si. Since ordering in the amorphous carbon film is limited to a very short distance, in the order of 2-3 the value of the lattice parameter (we can consider the hexagonal lattice of graphite or cubic diamond), the dynamic effects are negligible. The difference between intensities, as can be seen in Fig. 3a (left and right), cannot be ascribed to these effects. From Scherrer's analysis of the semi-height widths, crystal dimension of order 1,87 nm and 1,83 nm, respectively, as seen in Table 1. If we compare these values with the graphite lattice parameter (0.676nm) we get a ratio of about 2.75, and with that of the diamond (0.541nm) a ratio of about 3.5. These values confirm the presence of the amorphous film, possibly consisting of a mixture of graphite/diamond crystalline phases in small region (~2nm).

Fig. 2b features the TEM images for the Au sample. The Au sample was obtained by vacuum evaporation on the amorphous carbon substrate (e.g. commercially available as Quantifoil R1.2). From Scherrer's analysis of the FWHM calculated for the sample with gold nanoparticles, we obtain the crystals dimension of 6.9433 nm for the classical electron diffraction, and 6.9070 nm for electron diffraction pattern with precession system active, as seen in Table 1. The sample we are discussing here are crystalized particles, their sizes being observed in Fig. 2b, with values between 5 and 20 nm, forming clusters of particles in some places. It is a sample with monocrystalline and polycrystalline particles. On average, the size of nanocrystals can be considered around 7 nm. As we remark in Fig. 3b (left), the intensity of extracted profile is more intense in the case of data acquired using precession system. Relative intensities calculated from electron diffraction profiles in both cases are very close to XRD data (Fig. 3b right). Since the values corresponding to precession case are particularly almost identical with XRD (0.204nm and 0.124nm), we can conclude that we get a very good experimental example. Deviation for 0.144nm intensity ratio against XRD can be associated with incomplete background subtraction, automated algorithm used for this task are sensitive only to valley identified on profile.

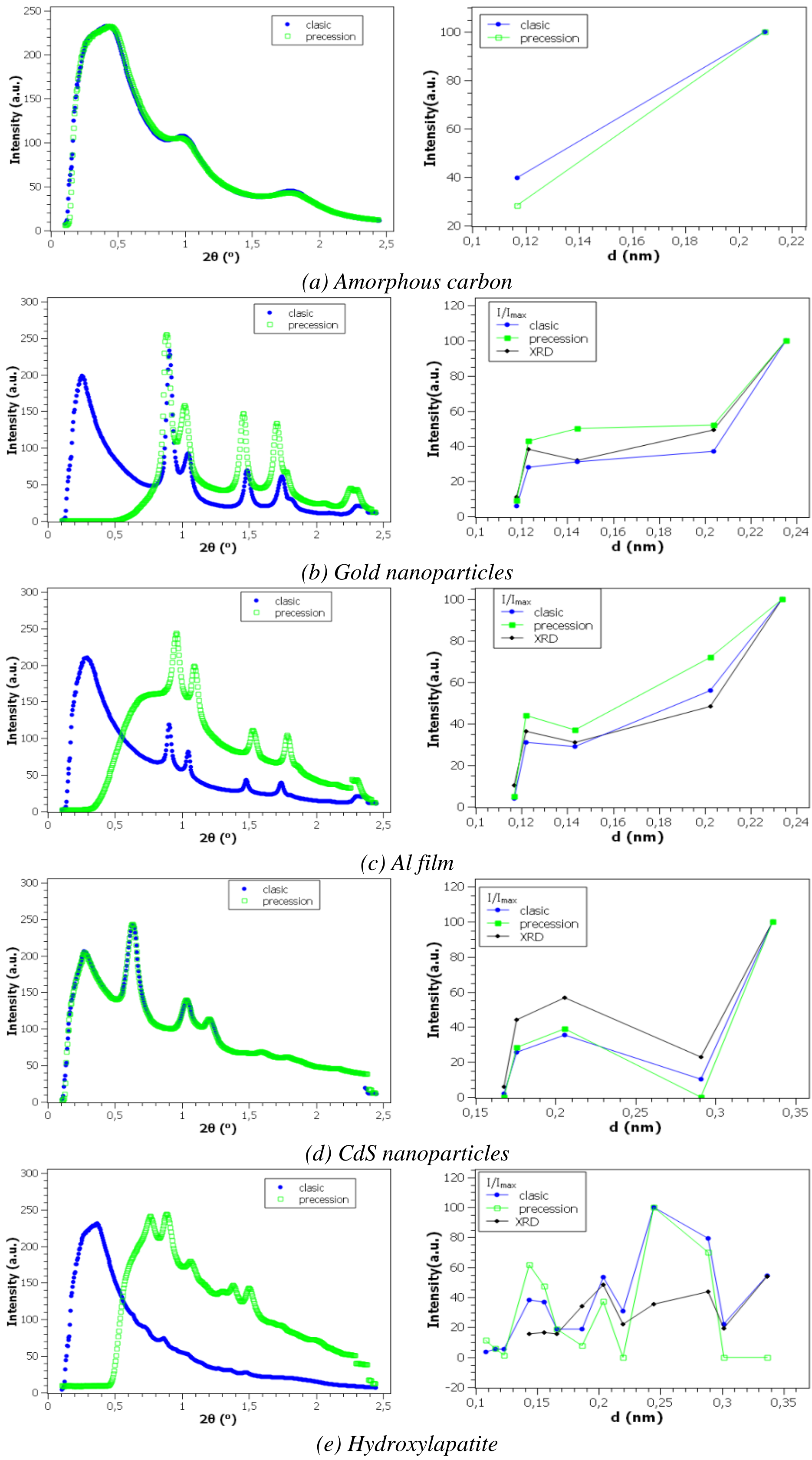

(a) Amorphous carbon

(b) Gold nanoparticles

(c) Al film

(d) CdS nanoparticles

(e) Hydroxylapatite

Fig. 3. Profiles extracted from diffraction figures (left) and evolution of the intensity of the peaks identified for classical diffraction, with precession system active and XRD (right).

Fig. 2c features TEM images of the film by Al polycrystalline, deposited by evaporation in vacuum on glass support. The preparation of the view grid was done by the quick method. Scherrer's analysis of the FWHM for the thin film Al, results in crystals dimension of 10.7974 nm for the classical electron diffraction and 6.9767 nm for the electron diffraction pattern with precession system active, as seen in Table I. The TEM image (Fig. 2c) show grains of thick Al film, with dimension spread over 10-100nm range. In Fig. 3c(left) we can compare intensity for both cases and comparing with XRD intensities ratio (Figure 3c right) we can conclude that same effect as in Au case appear. Classical data are close to XRD values, but ratio evaluated from data acquired using precession system are higher.

Fig. 2d features the TEM images for the CdS sample. For the Scherrer analysis we selected the first peaks identified and associated with the cubic structure of CdS. We can assume a mixture of cubic/hexagonal phases in this case. From Scherrer's analysis of FWHM results in crystals dimension of 4.46 nm for the classical electron diffraction and 3.76 nm for the electron diffraction pattern with precession system active, as seen in Table 1. We observe the same behavior as in the case of amorphous carbon film, here the ordering in the material is equivalent to the size of the nanoparticles. We can conclude in such cases that we are talking about a sample in which crystalline nanoparticles are monocrystalline. This case shows in Fig. 3d (left) no differences between profiles and comparing to XRD intensities ratio (Fig. 3d right) we get the same evolution but with smaller values for both cases.

Fig. 2e features TEM images of hydroxyapatite nanoparticles (HAp). The sample was obtained by chemical methods. From Scherrer's analysis of FWHM, crystalline areas of the order 6,05 nm for the classical electron diffraction and 5,37 nm for the electron diffraction pattern with precession system active, as seen in Table 1. The HRTEM image (Fig. 2e) show the crystallized particles of HAp, with dimensions in 10-20nm range. This experiment shows a very difficult case to analyze. One issue is impossibility to identify all peaks for precession case (Fig. 3e left) even profiles show higher intensities value compared with classical case. Also, the evolution of intensities ratio (Fig. 3e right) has a randomly behavior around XRD data. This can be ascribing to a complex structural and morphological sample. A multiphase system can’t be analyzed with such simple algorithm. To complete the task we can separate phases, keeping only the interest one and finally compared the results.

5. Conclusions

In conclusion, we can state that the precession method applied to electron diffraction, partially eliminates dynamic effects, especially multiple scatterings. From the cases studied, it is also noted that there are no significant differences for majority amorphous samples (C, CdS). In the case of crystalline samples, significant improvements in intensity are observed in the intensity of the peaks in the profiles extracted from the diffraction figure (Au, Al). In the case of these samples, there is a difference in the size of the estimated crystalline area of Scherrer's formula, thus for the nanoparticles of Au this difference is insignificant of about 0,5nm, but for Al where scattering may occur elimination by the precession system is also reflected in the size of the crystalline area determined in the Scherrer formula. Thus, for the classical electron diffraction we obtained a Scherrer size of 10,53nm, when activating the precession system this size decreased to 7,22nm.

The same effect occurs in the CdS nanoparticle sample (4.46nm and 3.57nm) and HAp nanoparticles (6.04nm and 5.37nm). In the case of the HAp sample, there are obvious difficulties in identifying the existing phases in the sample due to the background noise. This aspect also affects the proposed comparative analysis. In such situations, an alternative method for characterizing the material from a structural point of view is preferable. Analysis may be continued after the identification of the peaks of interest, without considering other phases of the sample.

Acknowledgements

The work has been founded by the Sectoral Operational Program Human Resources Development 2007 – 2013 of the Ministry of European Funds trough the Financial the Agreement POSDRU/159/1,5/S/137750.

References

[1] R. Vincent, P. A. Midgley, Ultramicroscopy **53**(3), 271 (1994).
[2] C. S. Own, L. D. Marks, W. Sinkler, Review of Scientific Instruments **76**, 033703 (2005).
[3] V. S. Teodorescu, M.-G. Blanchin, Microscopy and Microanalysis **15**(1), 15 (2009).
[4] S. Hovmöller, Ultramicroscopy **41**(1-3), 121 (1992).
[5] X. S. Zou, Ultramicroscopy **52**(3-4), 436 (1993).
[6] P. Scherrer, Nachrichten von der Gesellschaft der Wissenschaften zu Göttingen **26**, 98 (1918).
[7] J. W. Langford, A. J. C. Wilson, Journal of Applied Crystallography **11**, 102 (1978).
[8] (WWW-MINCRYST, GOLD-1780), (WWW-MINCRYST, ALUMINIUM-136), (WWW-MINCRYST, GREENOCKITE-1802), (WWW-MINCRYST, HAWLEYITE-1881), (WWW-MINCRYST, HYDROXYLAPATITE-2086)
[9] E. J. Kirkland, Advanced Computing in Electron Microscopy, Springer US, New York, p. 248, 2010.